Evaluation on Eddy Current Test Probe Performance

Reyhan Zuhdi Aditama[1] Samsudi Rahardjo[2,*] Dini Cahyandari[3]
[1,2,3]Universitas Muhammadiyah Semarang, Semarang, Central Java 50273, Indonesia
samraharjo@unimus.ac.id

Abstract. Eddy current non destructive test (ECT) were used for decades to assess magnetic conductive materials considering its reliability and its portability. The success of the ECT process mainly depends on the performance of the ECT's probe. The performance of the probe can be evaluated by applying frequency swept test which done by injecting a certain range of frequency to the probe and evaluate the reactance as the response of the probe. In this paper the fabricated helical probe is evaluated to assess its performance. From the test, the probe will work properly when the injected frequency range from 100 kHz to 1 MHz, and by calculation probe has depth penetration capability of 12.77 mm with excellent capability to perform as the probe of eddy current non destructive test.

Keywords: ECT, Probe, Impedance, Probe Geometry, Resonance Frequency.

1. Introduction

The magnetic methods had proved to be the most reliable methods on assessing magnetic conductive materials. According to to Wang et.al., the magnetic methods of NDT categorized into three categories i.e. magnetic flux leakage (MFL), magnetic Barkhaussen noise (MBN) and metal magnetic memory (MMM) [1]. Most of those forementioned methods works based on the evaluation of the electromagnetic stress distribution in the target. The most popular methods between those three that is constantly in the development process is the MFL. The uses of the MFL had varied from assessing the discontinuity of the material to the assessment of the coatings, and even nowadays are used to assessing the integrity of nonconductive material such as polymer by implanting conductive materials into the target of assessment first [2]–[7].

The eddy current test (ECT) that falls into the MFL category works by inducing electromagnetic to a conductive targets and some of the induced electromagnetic flows and exist at the surface of the target. These electromagnetic flux that strayed at the surface of the target is then detected. The detection process when the electromagnetic interact to the detection coil is manifested as the change of the impedance on the detection system [8]. The advantages of the ECT compared to other magnetic methods in assessing conductive targets

I. Yustar Afif and R. Nindyo Sumarno (eds.), *Proceedings of the 2nd Lawang Sewu International Symposium on Engineering and Applied Sciences (LEWIS-EAS 2023)*, Advances in Engineering Research 234,
https://doi.org/10.2991/978-94-6463-480-8_4

are: simple structure, compact size, insensitive to dirt (dust, oil, humid, dielectric material), etc [9]

The ECT system consist of three elements, i.e. the driving system, the detection system, and the target of the assessment [8]–[10]. The induction and detection of electromagnetic flux process were performed by a probe which consist of a driving coil system and a detection coil system. As by the name of the coils, the inductive section was handled by the driving coil, and the detection section were served by the detection coil. The wave generation were supplied from a wave or a function generator, and the detection coil were connected to a display system that displays the level of the electromagnetic signal that detected by the detection coil.

The success of the ECT were depend on several parameters, but the probe holds the greatest consideration. The placement of the probe on the target, the probe design, and the probe geometry handles the most important role of the assessment. The probe has to meet several condition i.e. have to be able to distribute the induced electromagnetic evenly to the target, to be able to monitor the change of phase and magnitude of the induced magnetic due to the presence of irregularity in the target, since the ECT works by measuring the change of the impedance of the probe, as the probe swept the target, etc.

There are several standard about the ECT, such as ISO 1763 about the crack [11], ASTM E-3052 about the probe lift-off and the range of injected signal [12], ASME about the data interpretation [13], and the TWI about the calibration [14]. According to the standard, the benchmark of the ECT were developed by several bodies, and the most widely adhered to testing electromagnetic analysis method (TEAM) and world federation of NDE centers (WFNDEC). These benchmark had common things on performing the ECT, i.e the change of the impedance as the probe approach the location of interest in the specimen.

In this paper, the performance of an ECT probe were characterized, specially to assess the crack on the conductive test piece. The performance of the probe were measured as the ability of the probe to respond to the change of impedance related to the induced electromagnetic to the target.

2. Probe Design

The design of the probe for the ECT in this experiment uses two coils, namely detection coil and the driving or the injection coil. the calculation is based on the theoretical model to calculate the coil impedance and it simplified to a cylindrical coil with an air core. This coil is modeled to be above the infinite test piece. Based on the finite element modeling,

the finite element of ECT is constructed. Then the impedance of the coil and the distribution of the magnetic flux were determined [15].

When designing the probe, the understanding of the modeling basic of the ECT system needs to be comprehended. The simple ECT works is shown in Figure 1.

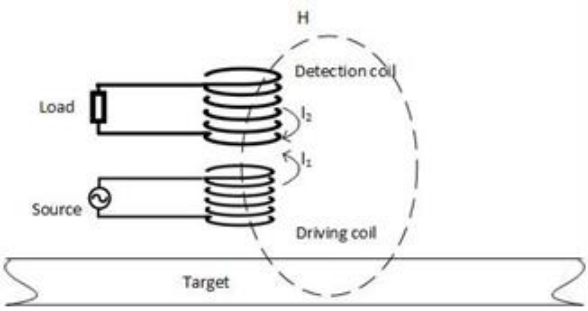

Fig 1. The depiction of an ECT system

The ECT simply consist of three elements i.e. detection, driving or injection, and target or the testpiece. The detection system usually consist of one or more detection coil and a display system that displays the detected signal level. The driving system or an injection system consist of one or more coil that connected to a wave generator to induct electromagnetic to the target. The target is the object of interest where the assessment is to be performed. When the electromagnetic energi induced to the target, the permeability of the target will alters the induced signal that will be detected by the detection signal.

The construction of the model is aimed to acquire the impedance of the coil and according to the Dodds and Deeds scheme, for the case of a cylinder of coils with rectangular cross section placed above a half space plate with conductivity α and permebility of the magnet μ_r with the geometry of axis symmetry is formulated as follow [16]:

$$Z = \frac{j\omega 2\pi}{I} \frac{N}{cross\ section} \iint_{cross\ section} rA_\varphi \, drdz \qquad (1)$$

This equation is based on the symmetric geometry depiction shown below:

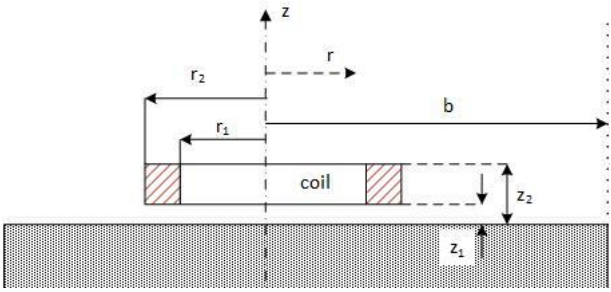

Fig 2. Dodd and Deeds model of an axisymmetric coil above the conductive plate

If the impedance of the coil is the sum of the impedance of air $(Z_0)$and the change of impedance (ΔZ), so for the half space axisymmetric [17]:

$$Z_0 = \frac{j\omega 2\pi\mu_0 N^2}{(r_2 - r_1)^2(z_2 - z_1)^2} \int_0^\infty \frac{Int^2(qr_1, qr_2)}{q^5} \times \left((z_2 - z_1) + \frac{\exp[-q(z_2 - z_1)] - 1}{q}\right) dq \quad (2)$$

and

$$\Delta Z = \frac{j\omega 2\pi\mu_0 N^2}{(r_2 - r_1)^2(z_2 - z_1)^2} \int_0^\infty \frac{Int^2(qr_1, qr_2)}{q^5} \times \left(\frac{[\exp(-qz_1) - \exp(-qz_2)]\text{^}2}{q^6}\right) \frac{q\mu_r - p}{q\mu_r + p} dq \quad (3)$$

where

$$Int(x_1, x_2) = \int_{x_1}^{x_2} xJ_1(x)dx \quad (4)$$

In (1)-(4) where N is the number of the turn of the coil, I is the excitation current, A_ϕ is the component of the magnetic potential and with $p = \sqrt{q^2 + j\omega\mu_r\mu_0\sigma}$ and $J_1(x)$ is the first kind and first order of the Bessel function. From Figure 2 by assuming that the region in which $b \to \infty$ lies is solution of the infinity region and by the serparation of the variables in Dirichlet condition of the magnetic field at $r = b$, we can write the general expression foer the magnetic vector potential as:

$$A_\phi(r,z) = \sum_{i=1}^{\infty} J_1(qir)[C_1 \exp(-p_i z) + D_i \exp(p_i z)] \tag{5}$$

where $p_i = \sqrt{q_1^2 + j\omega\mu_r\mu_0\sigma}$

the eigen value for the $q_i$is acquired from:

$$J_1(q,b) = 0 \tag{6}$$

or

$$J_1(x_i) = 0 \quad ; \quad q_i = \frac{x_i}{b} \tag{7}$$

So, the expression for the Dirichlet condition are the expansion of C_i and $D_i$and acquired by calculate the interface condition between the problem geometry and applying orthogonal part of the Bessel function. The impedances can be acquired by calculating the magnetic vector potential, and the final equation of the impedances are as follow:

$$Z_0 = \frac{j\omega 2\pi\mu_0 N^2}{(r_2 - r_1)^2(z_2 - z_1)^2} \sum_{0}^{\infty} Int^2(q_i r_1, q_i r_2) \times \frac{2[q_i(z_2 - z_1) - 1 + \exp[-q(z_1 - z_2)]}{[(q_i b)J_0(q_i b)]^2 q_i^5} \tag{8}$$

$$\Delta Z = \frac{j\omega 2\pi\mu_0 N^2}{(r_2 - r_1)^2 (z_2 - z_1)^2} \sum_{0}^{\infty} Int^2(q_i r_1, q_i r_2) \times \frac{[\exp(-q_i z_1) - \exp(-q_i z_2)]^2}{[(q_i b) J_0(q_i b)]^2 q_i^5} \frac{q\mu_r - p}{q\mu_r + p} \quad (9)$$

3. Methods

The proposed probe consists of the driving coil and a detection coil with air core with coplanar structure of coils depicted in Figure 3. The bobbin which consist of a cylinder core and a casing were made of a 25 mm diameter nylon cylinder, reduced to 9 mm by lathe process. The center of the bobbin was bored with 7 mm bore so the thickness of the bore center is 2 mm. The coils were coiled with a conventional coiling machine with a coiling counter. The driving coil placed and glued to the bobbin. The detection coil attached to the outer side of the driving coil, insulated by a solidified polymer glue. The wire is 0.2 mm laminated copper wire for either the driving and the detection coils. The casing was also made of a nylon cylinder, bored and lathed to fit the covering purpose of the probe. The parameter of the probe shown in the Table 1 The inductance and the capacitance of the probe listed in Table 2 were acquired by measurements using a LCR meter. The fabricated probe shown in Figure 4.

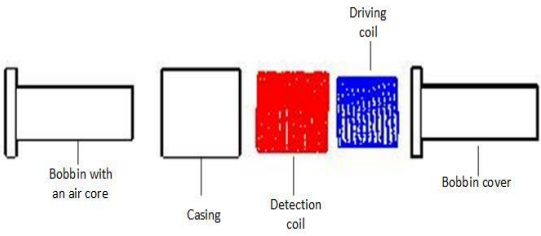

Fig 3. The design of the probe

Fig 4. The fabricated probe for this experiment

The frequency swept performed by using a tank circuit as shown in Figure 5 that shows the circuit diagrams (a) and the physical representatives (b) of the tank circuit arranged in a trainer board. The induction of the electromagnetic to the driving coil using RIGOL DG 1022 arbitrary wave generator, and the for the detection system, the RIGOL DS 1054Z oscilloscope were used. The injected wave is sinusiodal wave, with 8V and frequency from 100 Hz to 1MHz. The inductance measurements will be done in 21 measurements on the range of the formentioned frequency. The experimental configuration is shown in Figure 6.

Table 1. Geometric parameter of the probe

Parameter	Driving coil	Detection coil
Outer Diameter (mm)	22	24
Internal Diameter (mm)	12	22
Height (mm)	5	3
Turns	304	600

Table 2. The parameter of the probe according to the measurement

Coil	Parameter	Direct Probe	Planar Probe	Unit
Injection	Inductance, L_0	25.97	4.3	mH
	Resistance	3.8	1.7	Ω
	Capacitance	235	97	pF
Detection	Inductance, L_0	25.97	15	µH
	Resistance	5.51	2	Ω
	Capacitance	235	25	pF
	Coil outer radius	25	25	mm

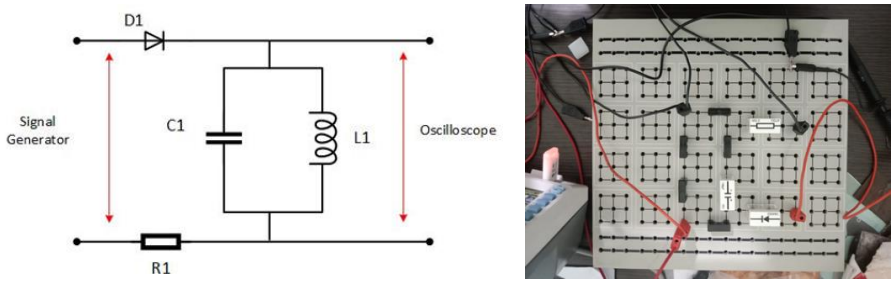

(a) (b)

Fig 5. Tank circuit (a) circuit diagram and (b) tank circuit assembled on a trainer board

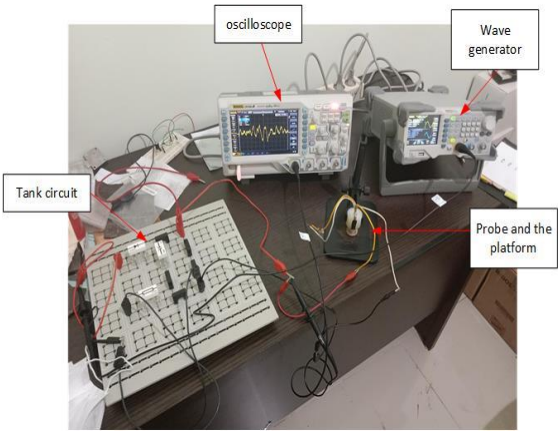

Fig 6. Experimental configuration

The probe was hanged on a platform, sets away from any conductive material that might affecting the measuring process. The process of measuring the frequency swept is shown in Figure 7. The data collection is taken from the oscilloscope. In the oscilloscope, the measurement provided was the frequency, as shown in the Figure 8. Since the data of interest are the induction, so to convert from the frequency, the resonant frequency formula is used. Since the quantity of the capacitor used in the circuit is known, it was easy to calculate the induction of the probe.

Fig 7. The free probe in inductance experiment

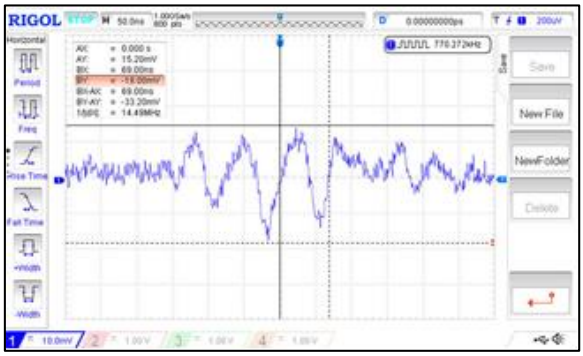

Fig 8. Example of the display of the oscilloscope

4. Results and Discussion

The plot of the injected frequency vs the impedance shown in Figure 9.

From the result of the frequency swept in Figure 9, it can be concluded that in the lower frequency below 1 kHz, the output impedance of the probe is weak, but it is linear to the injected frequency, shows that the real part and the imaginary part of the impedance were proportional. For the range of 1 kHz up to 10^5 Hz the impedance increment also proportional to the injected signal, but in a small proportion and tends to form a straight horizontal line indicating inductive reactance of the probe takes the main role of the reaction to the injected frequency. In the region above 10^5 Hz, the capacitive reactance takes places, indicated by at the same frequency on injection, the impedance is increasing, forms a vertical saturated lines in the graph. The capacitive response indicates that the storage of energy as the

characteristic of the capacitance takes places in the probe. We must note that the capacitive reactance will occurs at high frequency [18]. The capacitive reactance will cause significant delaying of electromagnetic flux induction, causing the inconsistency of the formed magnetic field, yields the bend of electromagnetic flux and even discontinued or breaking flux lines that will affect the result of the probe performance when the probe used for assessment. These region of frequency range (above 10^5) is not safe for measurements, since the probe will experience perturbation and attenuation [18]. The injected coils show the same characteristics as the detection coil with the smaller frequency span. This discrepancy cause by the lesser number of coil turns in the injection coil. It also means that the detection coil is more capable to receive the electromagnetic signal because it had bigger frequency range compared to the injection coil. This characteristic is required for an ECT probe to work properly.

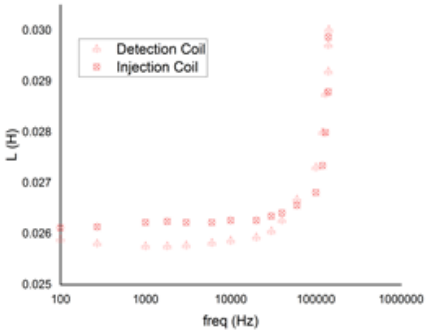

Fig 9. The frequency swept experiment result

From Figure 10, it is obvious that by using the ratio of the normalized impedance to the inductive reactance we can see that the transmission of the signal from the injection coil to the detection coil will experience almost no mismatch between the two coils, meaning that the detection process will detect almost the same value as the injecting value induced to the target on the safe frequency of measurement mentioned above.

From the calculation of the probe geometry according to (8) and (9), for the lift-off tabulated in Table 2, the maximum thickness of the target is 12.77 mm. the radius of the probe had no significant effect to the capability of the probe to penetrate to the certain depth and usually treated as an additional parameters [19]. From both (8) and (9), the geometry in the z direction had significant parameter in determining the depth of penetration in the target. The conductivity of the target also anulled in the computation since conductivity is a function of ϕ or only works in the ϕ direction in which by the magnetic vector potential calculation, the ϕ doesn't count.

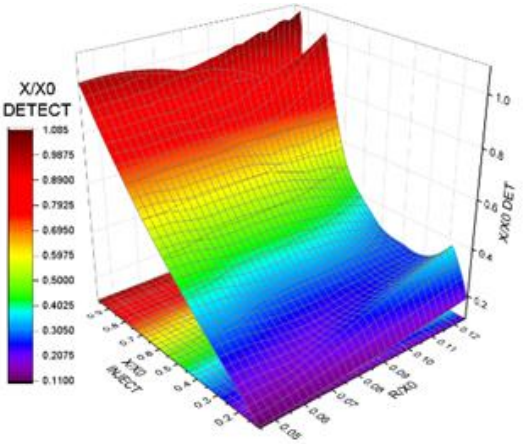

Fig 10. Plot of real part vs imaginary part of the injection and the detection coil

Author's Contributions

Reyhan and Samsudi carried out the experiment and wrote the manuscript with support from Dini.

Acknowledgments

This work has been supported by Universitas Muhammadiyah Semarang

References

1. Z. D. Wang, Y. Gu, and Y. S. Wang, "A review of three magnetic NDT technologies," *J. Magn. Magn. Mater.*, vol. 324, no. 4, pp. 382–388, 2012, doi: 10.1016/j.jmmm.2011.08.048.
2. D. Wu, F. Cheng, F. Yang, and C. Huang, "Non-destructive testing for carbon-fiber-reinforced plastic (CFRP) using a novel eddy current probe," *Compos. Part B Eng.*, vol. 177, no. September, p. 107460, 2019, doi: 10.1016/j.compositesb.2019.107460.
3. A. C. Lahrech *et al.*, "Development of an axial rotating magnetic field multi-coil eddy current sensor for electromagnetic characterization of stratified CFRP materials," *NDT E Int.*, vol. 126, p. 102589, 2022, doi: https://doi.org/10.1016/j.ndteint.2021.102589.
4. D. Wu, F. Cheng, F. Yang, and C. Huang, "Non-destructive testing for carbon-fiber-

reinforced plastic (CFRP) using a novel eddy current probe," vol. 177, no. April, 2019.
5. D. Berger, T. Will, H. C. Töpper, G. Lanza, D. Koster, and H. G. Herrmann, "Characterisation and Optimization of in-process Eddy Current Sensor Arrays Using Computed Tomography," *Procedia CIRP*, vol. 66, pp. 243–248, 2017, doi: 10.1016/j.procir.2017.03.363.
6. D. Berger, T. Will, H. C. Töpper, G. Lanza, D. Koster, and H. G. Herrmann, "Characterisation and Optimization of in-process Eddy Current Sensor Arrays Using Computed Tomography," *Procedia CIRP*, vol. 66, pp. 243–248, 2017, doi: 10.1016/j.procir.2017.03.363.
7. K. Mizukami *et al.*, "Enhancement of sensitivity to delamination in eddy current testing of carbon fiber composites by varying probe geometry," *Compos. Struct.*, vol. 226, no. July, 2019, doi: 10.1016/j.compstruct.2019.111227.
8. A. Sophian, G. Y. Tian, D. Taylor, and J. Rudlin, "Electromagnetic and eddy current NDT: A review," *Insight Non-Destructive Test. Cond. Monit.*, vol. 43, no. 5, pp. 302–306, 2001.
9. A. Aoukili and A. Khamlichi, "Modeling an Eddy-Current Probe for Damage Detection of Surface Cracks in Metallic Parts," *Procedia Technol.*, vol. 22, pp. 527–534, 2016, doi: https://doi.org/10.1016/j.protcy.2016.01.112.
10. A. Aoukili and A. Khamlichi, "Modeling an Eddy-Current Probe for Damage Detection of Surface Cracks in Metallic Parts," *Procedia Technol.*, vol. 22, pp. 527–534, 2016, doi: 10.1016/j.protcy.2016.01.112.
11. A. T. Smith, C. R. A. Schneider, C. R. Bird, and M. Wall, "Use of non-destructive testing for engineering critical assessment: Background to the advice given in BS 7910:2013," *Int. J. Press. Vessel. Pip.*, vol. 169, pp. 153–159, 2019, doi: 10.1016/j.ijpvp.2018.11.016.
12. ASTM E3052-21, "Standard Practice for Examination of Carbon Steel Welds Using An Eddy Current Array," *ASTM*, 2021. https://www.astm.org/e3052-21.html
13. ASTM, "Standard Practice for Examination of Carbon Steel Welds Using Eddy Current Array," *ASTM org*, 2021. https://www.astm.org/e3052-16.html
14. TWI, "EDDY CURRENT TESTING," *The Welding Institute*, 2022. https://www.twi-global.com/technical-knowledge/job-knowledge/eddy-current-testing-123#StandardsandCalibration
15. Y. Yu and P. Du, "Two approaches to coil impedance calculation of eddy current sensor," *Proc. Inst. Mech. Eng. Part C J. Mech. Eng. Sci.*, vol. 222, no. 3, pp. 507–515, 2008, doi: 10.1243/09544062JMES395.
16. D. J. Harrison, L. D. Jones, and S. K. Burke, "Benchmark problems for defect size and shape determination in eddy-current nondestructive evaluation," *J. Nondestruct. Eval.*, vol. 15, no. 1, pp. 21–34, 1996, doi: 10.1007/BF00733823.
17. T. Theodoulidis and E. Kriezis, "Series expansions in eddy current nondestructive evaluation models," *J. Mater. Process. Technol.*, vol. 161, no. 1-2 SPEC. ISS., pp. 343–347, 2005, doi: 10.1016/j.jmatprotec.2004.07.048.
18. J. I. Agbinya, *Wireless Power Transfer 2nd Edition*. 2016.

19. L. Barbato, N. Poulakis, A. Tamburrino, T. Theodoulidis, and S. Ventre, “Solution and Extension of a New Benchmark Problem for Eddy-Current Nondestructive Testing,” *IEEE Trans. Magn.*, vol. 51, no. 7, 2015, doi: 10.1109/TMAG.2015.2406765.